On behalf of my coauthors, I would like to thank the reviewers for their careful reading and constructive comments. We appreciate their recognition of the need for contact-freezing measurements and of the value of our new C-ICE experimental approach. The reviewers did raise important questions regarding the validation of contact freezing and the possible contribution of immersion freezing. These comments motivated several additional experiments and analyses that have substantially strengthened the manuscript.

In particular, we have added C-ICE experiments using soluble ammonium sulfate particles as a mode-specific validation of impact-initiated contact freezing, direct post-melt observations of quartz particles to independently evaluate particle collection, and AgI immersion freezing experiments to assess the potential contribution of immersion freezing. We believe that these additions, together with the corresponding revisions to the experimental description and interpretation, have significantly improved the manuscript.

Below we address each reviewer comment point by point. The reviewer comments are shown in blue, our responses in black, and the revised manuscript text in green. Line numbers refer to the revised manuscript, and the corresponding changes are highlighted in the revised version.

Referee #1

In this manuscript, Chen et al. introduce the C-ICE system, a novel cold-stage setup to measure impact-initiated contact freezing. This instrument is designed to enable the controlled, repeatable, and size-resolved investigation of contact freezing triggered by particle-droplet collisions.

The setup consists of a single 1 ml droplet deposited on a hydrophobic glass substrate mounted on a temperature-controlled cold stage that is cooled at a rate of 1 K/min. Particles are provided by a cooled and dehumidified particle-laden airflow that impinges on the droplet at a jet velocity of 4.0 m/s. Freezing is detected optically using a CCD camera through breath figure and grayscale analysis.

To constrain the collision efficiency (CE), the authors combine theoretical formulations of Brownian motion, inertial impact, interception, thermophoresis, diffusiophoresis, and electric forces with experimental estimates based on the assumption that a single collision triggers ice nucleation. To test C-ICE, silver iodide was used.

Overall, the manuscript is well-written, logically structured, and falls within the scope of AMT. However, different aspects of the setup, data analysis and interpretation are problematic and require clarification. These issues need to be addressed and revised before publication in AMT can be considered.

Author's response: We appreciate the referee's positive assessment of the manuscript and the constructive comments. To address the concerns raised, we conducted several additional experiments, including C-ICE measurements with soluble ammonium sulfate particles, AgI immersion freezing experiments, and post-melt quartz observations to independently evaluate particle collection. We also expanded the experimental description and revised the interpretation of freezing mode and collision efficiency. These additions have substantially strengthened the manuscript, as detailed below.

Major Comments:

The experimental setup should be explained in more detail. Specifically, the following points need to be addressed:

1. How is the relative humidity within the stage controlled during a cooling ramp? There is likely water

vapor condensation onto the droplet due to the supersaturation that is generated by cooling. Vapor condensation would heat the droplet surface and hamper the temperature accuracy of the experiment.

We thank you for raising this point. We agree that the relative humidity condition in the cold-stage chamber could be described more explicitly.

Although the chamber RH was not measured directly, our experimental observations indicate that the bulk environment of the C-ICE chamber remains subsaturated with respect to liquid water ($RH_w < 100\%$) during the measurements. Subsaturated conditions are maintained through two complementary measures. First, the particle-laden nitrogen stream is dehumidified and thermally conditioned before reaching the target droplet. Second, an additional dry nitrogen purge of 0.3 standard L min^{-1} is continuously introduced from the side of the cold stage chamber. Together, these flows maintain a subsaturated chamber environment during the cooling experiment.

This interpretation is supported by two experimental observations. First, the liquid droplet continuously decreases in size during cooling, indicating net evaporation rather than net condensation. This evaporation is particularly evident on the windward side of the droplet exposed to the impinging aerosol flow. Second, outside the spatially localized aerosol-flow-induced breath figure region, no persistent condensation droplets or breath figures are observed on the hydrophobic substrate before freezing. These observations are consistent with a bulk chamber environment that is subsaturated with respect to liquid water.

To clarify these points, we have added the chamber nitrogen purge flow to Sect. 2.1 and expanded the corresponding discussion of breath figure formation in Sect. 3.1.

"In addition, dry nitrogen is continuously introduced from the side of the cold-stage chamber at 0.3 standard L min^{-1} during the experiment. The combination of dehumidification of the aerosol stream and purging of the C-ICE chamber maintains the bulk cold-stage environment subsaturated with respect to liquid water and suppresses persistent background condensation during cooling." (Lines 130-133)

"Prior to freezing (Fig. 2c), introduction of the conditioned aerosol stream (white arrow) produces localized breath figures in the wake region of the droplet. We refer to these as aerosol-flow-induced breath figures (purple annotations), because they arise from the local temperature and water vapor perturbation associated with the impinging flow. These features are spatially localized. Outside this flow affected region, no persistent condensation is observed on the hydrophobic substrate before freezing." (Lines 300-304)

"Because the chamber remains globally subsaturated with respect to liquid water, these condensation features are transient and disappear as the local perturbation dissipates. Together with the grayscale response, the freezing-induced breath figures provide a robust optical indicator of the initiation of the liquid-to-ice phase transition." (Lines 319-322)

"The dehumidifier provides a reproducible and sufficiently dry thermodynamic state prior to particle delivery. Together with the continuous dry nitrogen purge of the cold-stage chamber, this conditioning suppresses widespread background condensation while allowing localized aerosol-flow-induced and freezing-induced breath figures to remain readily distinguishable." (Lines 407-410)

2. The role of the aerosol flow for the humidity within the chamber remains unclear. The manuscript describes the pre-cooling to -15°C within the dehumidifier in detail, but it does not become clear whether the temperature of the dehumidifier is kept at a constant temperature of -15°C or whether its temperature decreases together with the one of the stage. Moreover, it remains unclear at which temperature the aerosol stream is turned on. In the experiment that is displayed in Fig. 2, it was turned on at -11.5°C, i.e. shortly before the droplet froze. Was this always the case or was this especially done to illustrate that the breath figure is due to the aerosol stream? When it was usually turned on while the cooling ramp was already running: how did you decide when to turn it on? How long before freezing was it turned on usually?

We thank you for these comments. To clarify, the dehumidifier temperature is not coupled to the cold-stage cooling ramp. Its operating temperature is selected according to the aerosol material and experimental condition to provide sufficient drying and reproducible conditioning of the particle-laden nitrogen stream. Once selected for a given sample or experimental series, the dehumidifier temperature is held constant.

The -15 °C condition shown in Fig. 4 represents one illustrative operating scenario used to demonstrate the thermodynamic evolution of the aerosol stream through the dehumidifier; it should not be interpreted as the universal set point for all C-ICE experiments. We have revised the figure caption and the corresponding text to clarify this point.

The referee is correct that the aerosol stream is normally introduced only shortly before the anticipated freezing temperature range. This is an intentional feature of the C-ICE protocol. Delaying aerosol admission serves two purposes. First, it limits prolonged exposure of the droplet to the dry carrier gas flow and therefore minimizes excessive evaporation before the relevant freezing temperature range is reached. Second, it limits the cumulative number of particles collected by the droplet before freezing. Prolonged particle exposure, particularly together with a decreasing droplet volume, would increase the particle loading per unit liquid volume and thereby increase the potential contribution from delayed immersion freezing. Introducing the aerosol stream relatively close to the expected freezing range was therefore deliberately chosen to reduce this ambiguity.

The exact aerosol exposure start temperature is not identical for all materials because the characteristic freezing range depends strongly on particle characteristics. For each new material or experimental condition, preliminary measurements are first used to identify the approximate temperature range over which freezing is expected. The aerosol admission point is then selected so that particle delivery begins shortly before this range while allowing sufficient time for stable aerosol delivery and particle-droplet interactions. The same protocol is subsequently applied consistently within the corresponding experimental series. This sample dependent procedure has been refined through extensive operation of the C-ICE system, including more than one thousand independent freezing experiments to date. We have added the general operating principle to Sect. 2.1.

"The dehumidifier setpoint is selected according to the aerosol material, its expected freezing temperature range, and the required drying conditions. For a given sample or experimental series, the selected setpoint is held constant. This configuration allows both the aerosol particles and the nitrogen carrier gas to approach a selected target conditioning temperature before collision, while simultaneously reducing the water vapor content of the aerosol stream." (Lines 124-127)

"Note that the aerosol stream is not applied continuously throughout the entire cooling ramp. Instead, aerosol delivery is initiated shortly before the expected freezing temperature range of the material under investigation. The approximate freezing range is first established from preliminary experiments, after which a consistent aerosol admission protocol is used for the corresponding experimental series. This strategy limits prolonged exposure of the droplet to the dry aerosol flow and minimizes excessive droplet evaporation and cumulative particle loading before the relevant freezing temperature window. Limiting particle accumulation is particularly important for reducing the potential contribution from delayed immersion freezing by particles collected prior to the observed freezing event." (Lines 139-145)

"At the outlet, the aerosol particles and nitrogen carrier gas have been both dried and thermally conditioned toward the selected setpoint before entering the cold stage. Because the dehumidifier temperature is fixed during an experimental series while the cold-stage temperature continues to decrease, the conditioned aerosol stream is not necessarily at the same instantaneous temperature as the target droplet. The dehumidifier provides a reproducible and sufficiently dry thermodynamic state prior to particle delivery. Together with the continuous dry nitrogen purge of the cold-stage chamber, this conditioning suppresses widespread background condensation while allowing localized aerosol-flow-induced and freezing-induced breath figures to remain readily distinguishable." (Lines 404-410)

"Figure 4: …The simulation is performed for an inlet airstream at room temperature (25 °C), an initial RH of 10%, a flow rate of 1.5 L min^{-1}, and a representative dehumidifier coolant setpoint of -15 °C. The -15 °C condition illustrates one typical operating scenario and does not represent a universal setpoint for all C-ICE experiments. The dehumidifier temperature is selected according to the aerosol material, expected freezing temperature range, and drying requirements and is held constant within a given experimental series." (Lines 417-421)

3. What is the distance between the nozzle and the droplet? An air jet of 4.0 m/s should generate a vertical stagnation pressure and surface shear, which again might induce internal circulation within the droplet if the nozzle is placed close to the droplet surface. This needs to be discussed.

We thank you for this comment.

The nozzle-to-droplet distance is 5 mm and has now been added to Sect. 2.1. We also clarify that the reported 4.0 m s^{-1} corresponds to the mean gas velocity at the nozzle exit, not the local gas or particle velocity at the droplet surface.

We agree that the impinging jet can generate a stagnation region, surface shear, and internal circulation within the droplet, which may influence particle approach and post-contact redistribution. Quantitatively resolving these coupled gas- and liquid-phase processes would require a dedicated three-dimensional hydrodynamic simulation and is beyond the scope of the present analytical CE model.

For this reason, the physical CE model is used as a baseline rather than as a stand-alone prediction. Its magnitude is constrained experimentally using the 200 and 800 nm AgI measurements, and the revised manuscript further includes direct post-melt quartz observations as an independent check of particle collection in the actual C-ICE geometry.

"In this work, a nozzle orifice diameter of 0.8 mm, an aerosol flow rate of 120 cm^3 min^{-1}, and a nozzle-to-droplet distance of 5 mm were employed, corresponding to a mean gas velocity of 4.0 m s^{-1} at the nozzle exit. This configuration provides directed particle delivery to the target droplet, while the impinging flow may generate surface shear and internal circulation within the droplet. The resulting particle-droplet collision efficiency is quantified and discussed in Sects. 2.3 and 3.3." (Lines 135-139)

"In this section, we combine the physically based collision model described in Sect. 2.3 with experimental constraints from size-selected AgI measurements and direct observations of quartz particle features retained in the target droplet after freezing and melting to derive an observation-constrained collision efficiency for C-ICE." (Lines 438-440)

"This treatment yields median freezing-inferred CE constraints of 0.04 for 200 nm AgI (0.03-0.07, 25-75%; mean=0.05; n=29) and 0.10 for 800 nm AgI (0.07-0.15, 25-75%; mean=0.11; n=32; shown as black symbols in Figs. 5 and 6; Table S2). These values are treated as empirical constraints on the C-ICE collision efficiency rather than as direct measurements of individual particle trajectories. They are substantially higher than the corresponding CE_{model} values (9.7×10^{-5} for 200 nm and 0.01 for 800 nm), indicating that the collision model does not fully capture effective particle collection under the actual C-ICE geometry." (Lines 479-484)

Also, the data interpretation requires reconsideration:

4. The explanation that the breath figure is generated through aerosol-droplet collisions is highly unlikely or even impossible as the impact of 200 nm particles is not sufficient. A more likely explanation is that the breath figure is generated by the humidity within the chamber and/or in the aerosol flow. This again raises questions regarding the water vapor equilibration within the chamber and the aerosol flow.

We thank you for this suggestion.

We no longer attribute the pre-freezing breath figures to individual aerosol-particle impacts. Instead, they are described as aerosol-flow-induced breath figures, caused by local thermal and water-vapor perturbations associated with the impinging conditioned flow. At freezing onset, a second, spatially distinct condensation pattern appears abruptly; this freezing-induced breath figure is attributed to the transient thermal and vapor perturbation associated with latent-heat release. We have also clarified that the aerosol stream is dehumidified and the chamber is continuously purged with dry N2, maintaining a globally subsaturated environment outside the localized flow affected region.

"In addition, dry nitrogen is continuously introduced from the side of the cold-stage chamber at 0.3 standard L min^{-1} during the experiment. The combination of dehumidification of the aerosol stream and purging of the C-ICE chamber maintains the bulk cold-stage environment subsaturated with respect to liquid water and suppresses persistent background condensation during cooling." (Lines 130-133)

"Prior to freezing (Fig. 2c), introduction of the conditioned aerosol stream (white arrow) produces localized breath figures in the wake region of the droplet. We refer to these as aerosol-flow-induced breath figures (purple annotations), because they arise from the local temperature and water vapor perturbation associated with the impinging flow. These features are spatially localized. Outside this flow affected region, no persistent condensation is observed on the hydrophobic substrate before

freezing." (Lines 300-304)

"Because the chamber remains globally subsaturated with respect to liquid water, these condensation features are transient and disappear as the local perturbation dissipates. Together with the grayscale response, the freezing-induced breath figures provide a robust optical indicator of the initiation of the liquid-to-ice phase transition." (Lines 319-322)

"The dehumidifier provides a reproducible and sufficiently dry thermodynamic state prior to particle delivery. Together with the continuous dry nitrogen purge of the cold-stage chamber, this conditioning suppresses widespread background condensation while allowing localized aerosol-flow-induced and freezing-induced breath figures to remain readily distinguishable." (Lines 407-410)

5. The competition between contact and immersion freezing is not discussed at all in the manuscript. Considering, that the droplet constantly accumulates particles as soon as the aerosol flow is turned on, the immersion freezing probability increases as the AgI concentration in the droplet becomes higher. This needs to be discussed.

We thank you for pointing out this important comment.

We addressed this comment in three ways. First, aerosol delivery is intentionally initiated only shortly before the expected freezing range to limit cumulative particle loading. Second, we added a mode-specific validation using dry ammonium sulfate. The particles dissolve after entering the water droplet, so no persistent solid ammonium-sulfate surface remains to support conventional delayed immersion freezing, and the resulting solution would freeze homogeneously only at much lower temperatures. Third, we performed new AgI immersion-freezing experiments from 0.0001 to 1 wt% using the same cold-stage platform, 1 µL droplets, and 1 °C min^{-1} cooling rate. These measurements directly show that AgI immersion freezing is strongly concentration dependent. We therefore use AgI as a benchmark and do not treat it as the sole proof of freezing mode; ammonium sulfate provides the more direct mode-specific validation.

"Note that the aerosol stream is not applied continuously throughout the entire cooling ramp. Instead, aerosol delivery is initiated shortly before the expected freezing temperature range of the material under investigation. The approximate freezing range is first established from preliminary experiments, after which a consistent aerosol admission protocol is used for the corresponding experimental series. This strategy limits prolonged exposure of the droplet to the dry aerosol flow and minimizes excessive droplet evaporation and cumulative particle loading before the relevant freezing temperature window. Limiting particle accumulation is particularly important for reducing the potential contribution from delayed immersion freezing by particles collected prior to the observed freezing event." (Lines 139-145)

"Importantly, $(NH_4)_2SO_4$ provides a mode-specific validation of impact-initiated contact freezing in C-ICE. The dry crystalline particles dissolve after entering the pure water droplet, so no persistent solid ammonium sulfate surface remains to support conventional delayed immersion freezing. Once dissolved, ammonium sulfate lowers water activity and favors homogeneous freezing only at substantially lower temperatures. Consistent with this, Kohn et al. (2016) used $(NH_4)_2SO_4$ particles to form dilute cloud droplets and observed no heterogeneous freezing signal above 236 K (-37.15 °C),

with freezing occurring only in the homogeneous regime. This is approximately 20 °C colder than the -17.7 to -14.4 °C freezing range observed here. Thus, neither intrinsic background freezing nor homogeneous or delayed immersion freezing following particle dissolution can reasonably account for the observed warm temperature response. The $(NH_4)_2SO_4$ experiments therefore provide direct evidence that C-ICE can generate and detect impact-initiated contact freezing, while simultaneously demonstrating stable and reproducible system performance." (Lines 384-393)

"Silver iodide (AgI) was used as a benchmark material to further evaluate the freezing mode sensitivity and size-resolved performance of C-ICE. In addition to the contact freezing measurements, immersion freezing experiments were performed using the same cold stage and hydrophobic glass substrate. Following the droplet array approach used in Chen et al. (2021), 70 droplets of 1 µL AgI suspension were analyzed per experiment at the same cooling rate of 1 °C min^{-1} used in C-ICE. Frozen fractions and 95% confidence intervals were calculated using the Wilson score method in Eq. (2). A series of AgI suspensions from 0.0001 to 1 wt% was prepared to span and exceed the particle loading relevant to the polydisperse AgI contact freezing measurements. In C-ICE experiments, the upper-bound AgI mass concentration in the 1 µL target droplet was estimated from the OPC-measured particle size distributions assuming $CE_{upper}=1$, i.e., that all nozzle-delivered particles were collected. Assuming spherical particles with an AgI density of 5.68 g cm^{-3}, the resulting upper-bound concentration has a median of 0.0051 wt% and an interquartile range of 0.0037-0.0076 wt% (Table S3). The actual concentrations of the prepared immersion freezing suspensions are summarized in Table S4." (Lines 544-554)

"Figure 8 compares the frozen fraction behavior of AgI in immersion and impact-initiated contact freezing. For immersion freezing, the temperature of the first observed freezing event ranges from approximately -4.6 to -7.2 °C across the concentration series, warmer than the polydisperse AgI C-ICE response. However, the immersion freezing curves show a pronounced concentration dependence, shifting systematically toward lower temperatures as AgI concentration decreases. At 0.0001 wt%, the immersion T_{50} approaches that of the polydisperse C-ICE experiment. The corresponding pure-water/background curves are comparable, indicating that the differences among the AgI datasets arise primarily from particle exposure rather than from differences in the cold-stage baseline. A similar mode dependence was reported by Nagare et al. (2016), who observed that heterogeneous freezing of AgI in the CLINCH contact freezing experiments occurred at lower temperatures than in the corresponding IMCA-ZINC immersion experiments.

These results illustrate an important point for freezing mode comparison. When the immersion mode activity of a material is substantially weaker than its contact freezing response at comparable particle loading, freezing observed following aerosol-droplet interaction can be attributed more confidently to impact-initiated contact freezing. In contrast, for highly immersion active materials such as AgI, particles collected before the observed freezing event may contribute to the measured response, particularly as particle loading increases. Therefore, a rigorous quantitative comparison of intrinsic contact and immersion freezing efficiencies requires careful matching of particle loading, surface area, and particle-water interaction history. The AgI experiments presented here are intended primarily as a benchmark of C-ICE performance and as a direct assessment of the potential immersion contribution, rather than as a complete quantitative ranking of the two freezing modes. The ammonium sulfate experiments in Sect. 3.2 provide the more direct mode-specific validation of impact-initiated contact freezing.

The size-resolved AgI contact freezing measurements are summarized in Fig. 9. The 800 nm AgI particles froze at slightly higher temperatures (-12.7 to -11.5 °C, T_{50}=-12.0°C; n=34) than the 200 nm particles (-13.9 to -11.8 °C, T_{50}=-12.6°C; n=31) (Table S1). The polydisperse aerosol exhibits freezing at still higher temperatures and over a broader interval (-11.1 to -9.2 °C, T_{50}=-10.1°C; n=50), reflecting contributions from coarse-mode particles. The two size-selected populations also exhibit steeper frozen fraction slopes than the polydisperse case. These systematic differences under the same C-ICE geometry and thermodynamic conditions support a particle-size dependence of the AgI freezing response. The warmer freezing observed for 800 nm relative to 200 nm AgI is consistent with previous evidence that contact freezing efficiency depends strongly on particle size. Hoffmann et al. (2013a) reported a pronounced size dependence for size-selected illite particles, with larger particles exhibiting higher single-contact freezing probabilities. More broadly, AgI ice-nucleating activity is known to depend on available surface area and interfacial configuration (Marcolli et al., 2016). Larger particles may promote freezing through a combination of increased contact area, differences in collision/contact and wetting dynamics, and a higher probability of containing active nucleation sites. The present measurements do not isolate these mechanisms individually, but demonstrate that C-ICE can resolve particle size-dependent freezing behavior under controlled collision conditions." (Lines 562-592)

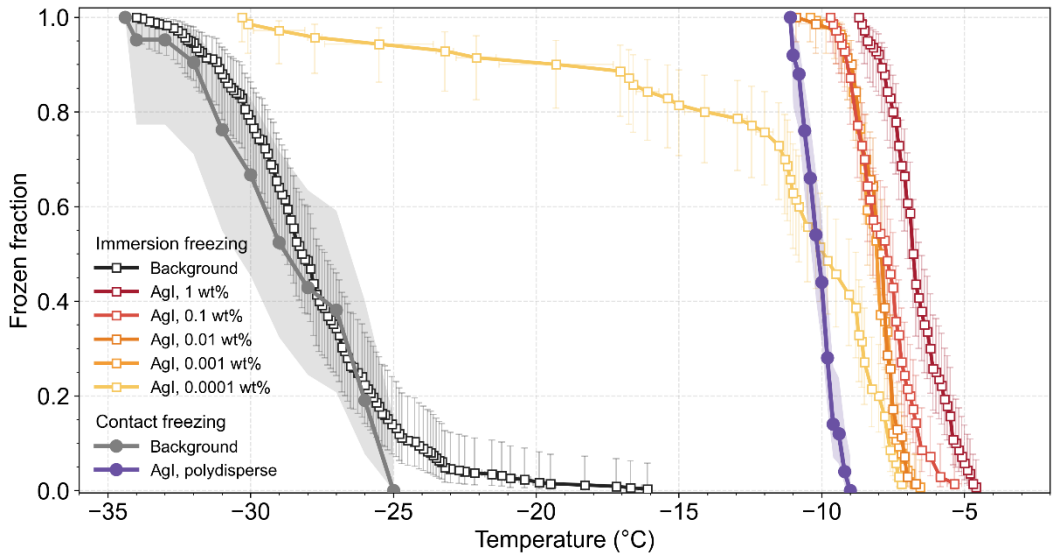


Figure R1.1. Comparison of AgI immersion and impact-initiated contact freezing. Frozen fraction as a function of temperature is shown for immersion freezing experiments using AgI suspensions spanning 0.0001–1 wt% (open symbols), polydisperse AgI impact-initiated contact freezing experiments in C-ICE (purple filled symbols), and the corresponding particle-free/background measurements. Immersion freezing experiments used 70 droplets of 1 µL per condition on the same cold-stage platform and at the same cooling rate as the C-ICE experiments. Error bars and shaded regions represent 95% confidence intervals calculated using the Wilson score method. Actual AgI suspension concentrations are listed in Table S4. (Fig. 8)

6. Considering the recent literature, immersion mode freezing is more efficient for AgI than contact freezing (Nagare et al. 2016; Marcolli et al., 2016). Marcolli et al. (2016) reported median immersion freezing temperatures of -9°C for 200 nm AgI particles for residence times of 10 s and -11°C for 3 s.

Both temperatures are above the median freezing onset temperature for contact freezing (-12.7°C) in C-ICE. A higher efficiency for immersion compared with contact freezing was also observed for 200 nm AgI particles by Nagare et al. (2016). These authors state that in their setup freezing was induced by single AgI particles collected by the droplets within the chamber. Considering that their freezing temperatures are well below the ones measured with C-ICE, immersion freezing on previous collected AgI particles is the more likely mechanism for the experiments performed in this study. This competition between immersion and impact-initiated contact freezing needs to be discussed adequately.

We agree that AgI is highly immersion active which the original version did not adequately address. The new immersion freezing measurements described above directly address the concern. Across our concentration series, the first immersion freezing events occur at approximately -4.6 to -7.2 °C, warmer than the polydisperse C-ICE response, consistent with the literature cited by the referee. However, the immersion curves shift strongly with concentration, and at 0.0001 wt% the immersion T_{50} approaches that of the polydisperse C-ICE experiment. Therefore, a quantitative ranking of intrinsic contact and immersion efficiencies requires careful matching of particle loading, surface area, and interaction history. We now state this explicitly and use AgI as a benchmark rather than as the mode-specific validation.

"Figure 8 compares the frozen fraction behavior of AgI in immersion and impact-initiated contact freezing. For immersion freezing, the temperature of the first observed freezing event ranges from approximately -4.6 to -7.2 °C across the concentration series, warmer than the polydisperse AgI C-ICE response. However, the immersion freezing curves show a pronounced concentration dependence, shifting systematically toward lower temperatures as AgI concentration decreases. At 0.0001 wt%, the immersion T_{50} approaches that of the polydisperse C-ICE experiment. The corresponding pure-water/background curves are comparable, indicating that the differences among the AgI datasets arise primarily from particle exposure rather than from differences in the cold-stage baseline. A similar mode dependence was reported by Nagare et al. (2016), who observed that heterogeneous freezing of AgI in the CLINCH contact freezing experiments occurred at lower temperatures than in the corresponding IMCA-ZINC immersion experiments.

These results illustrate an important point for freezing mode comparison. When the immersion mode activity of a material is substantially weaker than its contact freezing response at comparable particle loading, freezing observed following aerosol-droplet interaction can be attributed more confidently to impact-initiated contact freezing. In contrast, for highly immersion active materials such as AgI, particles collected before the observed freezing event may contribute to the measured response, particularly as particle loading increases. Therefore, a rigorous quantitative comparison of intrinsic contact and immersion freezing efficiencies requires careful matching of particle loading, surface area, and particle-water interaction history. The AgI experiments presented here are intended primarily as a benchmark of C-ICE performance and as a direct assessment of the potential immersion contribution, rather than as a complete quantitative ranking of the two freezing modes. The ammonium sulfate experiments in Sect. 3.2 provide the more direct mode-specific validation of impact-initiated contact freezing.

The size-resolved AgI contact freezing measurements are summarized in Fig. 9. The 800 nm AgI particles froze at slightly higher temperatures (-12.7 to -11.5 °C, T_{50}=-12.0°C; n=34) than the 200 nm particles (-13.9 to -11.8 °C, T_{50}=-12.6°C; n=31) (Table S1). The polydisperse aerosol exhibits freezing

at still higher temperatures and over a broader interval (-11.1 to -9.2 °C, T_{50}=-10.1°C; n=50), reflecting contributions from coarse-mode particles. The two size-selected populations also exhibit steeper frozen fraction slopes than the polydisperse case. These systematic differences under the same C-ICE geometry and thermodynamic conditions support a particle-size dependence of the AgI freezing response. The warmer freezing observed for 800 nm relative to 200 nm AgI is consistent with previous evidence that contact freezing efficiency depends strongly on particle size. Hoffmann et al. (2013a) reported a pronounced size dependence for size-selected illite particles, with larger particles exhibiting higher single-contact freezing probabilities. More broadly, AgI ice-nucleating activity is known to depend on available surface area and interfacial configuration (Marcolli et al., 2016). Larger particles may promote freezing through a combination of increased contact area, differences in collision/contact and wetting dynamics, and a higher probability of containing active nucleation sites. The present measurements do not isolate these mechanisms individually, but demonstrate that C-ICE can resolve particle size-dependent freezing behavior under controlled collision conditions.

The AgI freezing temperatures observed here are also comparable with previously reported values. Submicron AgI particles in C-ICE initiate freezing near -12 °C, comparable to earlier CLINCH measurements (Nagare et al., 2016). At the other end of the size range, Schiffman et al. (2025) reported surface-initiated contact freezing by large AgI particles (~380 μm) with a mean freezing temperature of -5.4 ± 1.1 °C, substantially warmer than the submicron aerosol results reported here. Earlier experimental studies similarly reported AgI contact freezing temperatures spanning from approximately -5 °C to -25 °C, depending on particle size, droplet size, aerosol loading, and experimental configuration (Gokhale and Goold, 1968; Sax and Goldsmith, 1972; Langer et al., 1978; DeMott, 1995; Nagare et al., 2016). Together, these studies emphasize that AgI contact freezing is strongly dependent on particle and experimental conditions rather than being characterized by a single freezing temperature." (Lines 562-601)

7. The authors write at several instances in the manuscript (e.g., lines 417–425 and 505–509) that relying on the assumption that each freezing event corresponds to an impact, a lower limit for the collision efficiency can be obtained. Yet, considering that freezing likely occurs in immersion mode on previously accumulated droplets, the collision efficiency might even be lower. Thus, the freezing data can neither provide an upper nor a lower constraint.

We appreciate your comment.

The previous "lower-bound" terminology has been removed. Equation (12) is now described as yielding a freezing-inferred experimental efficiency, CE_{exp}, under the stated one-effective-collision assumption. These values are used as empirical constraints, not as direct trajectory measurements and not as unconditional lower bounds. We now distinguish CE_{model}, CE_{exp}, $CE_{upper} = 1$, and CE_{constr}. In addition, the post-melt quartz experiments provide an independent evaluation of particle collection that does not depend on the freezing response itself.

"These values are treated as empirical constraints on the C-ICE collision efficiency rather than as direct measurements of individual particle trajectories. They are substantially higher than the corresponding CE_{model} values (9.7×10^{-5} for 200 nm and 0.01 for 800 nm), indicating that the collision model does not fully capture effective particle collection under the actual C-ICE geometry." (Lines 481-484)

"To reconcile model predictions with experimental constraints, we define three CE scenarios in Figs. 6 and S7. CE_{model} represents the physically modeled collision efficiency without observational adjustment. CE_{upper} represents the idealized upper limit in which all nozzle-delivered particles collide with the target droplet. The observation-constrained collision efficiency, CE_{constr}, incorporates the experimentally derived constraints at 200 and 800 nm while retaining the physical size dependence predicted by the model." (Lines 497-501)

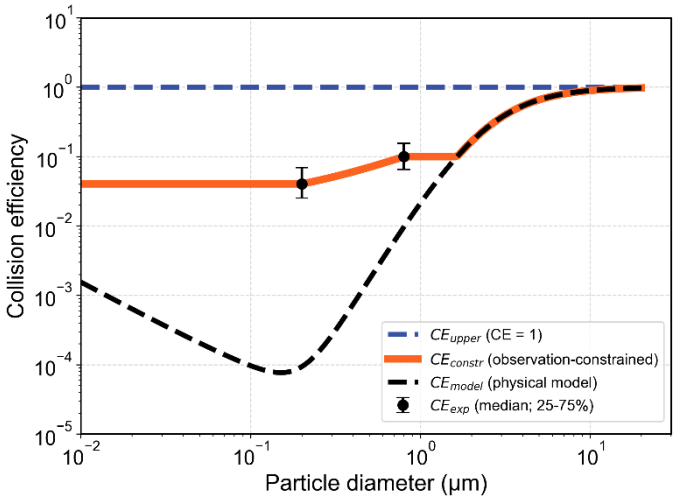


Figure R1.2. Modeled, upper-bound, and observation-constrained collision efficiencies for the C-ICE system. The physically modeled collision efficiency (CE_{model}, dashed black line), the idealized upper bound assuming unit collision efficiency (CE_{upper}=1, dashed blue line), and the observation-constrained collision efficiency (CE_{constr}, solid orange line) are shown as a function of particle diameter. CE_{constr} is constructed by combining the physical size dependence represented by CE_{model} with the experimentally inferred CE_{exp} constraints at 200 and 800 nm. Black circles indicate CE_{exp}, shown as the median with interquartile range (25-75%). (Fig. 6)

"To independently evaluate particle collection without relying on the freezing response itself, additional C-ICE experiments were conducted using quartz particles. For DMA selected 800 nm quartz particles, numerous optically resolved quartz features were observed within the droplet after freezing and subsequent melting (Fig. S8), directly confirming substantial particle collection under the actual nozzle-droplet geometry. A separate experiment with polydisperse quartz particles similarly revealed a large population of retained particles. Automated image analysis identified 3046 particle features within the post-melt droplet (Fig. S9)." (Lines 519-524)

Taking all these issues together, running C-ICE in continuous cooling mode leads to uncontrolled conditions with respect to droplet surface temperature and precludes the accurate determination of the freezing temperature when it is initiated at the particle surface. Moreover, an unambiguous identification of the freezing process as impact-initiated contact freezing is not possible when there is competition with immersion freezing.

Discrimination between immersion and impact-initiated contact freezing might be possible when experiments were performed at constant temperature. The range of temperatures of interest could first be

narrowed down in a cooling cycle. Subsequently, the two freezing modes could be discriminated with an off/on sequence of the aerosol flow at constant temperature. When the freezing probability is independent of the presence/absence of the aerosol flow, impact-initiated contact freezing can be excluded.

We thank you for this suggestion. However, rather than replacing the continuous-cooling protocol, we directly address the underlying mode ambiguity with independent controls: (i) aerosol exposure is restricted to the relevant temperature window; (ii) ammonium sulfate provides a soluble-particle mode-specific test; (iii) AgI immersion freezing is measured directly across five concentrations; and (iv) direct observations of quartz particles retained in the target droplet provide an independent evaluation of particle collection. Continuous cooling is retained because it provides temperature-resolved frozen fraction curves under a consistent cooling protocol. We have correspondingly narrowed our claims: AgI is treated as a benchmark for C-ICE performance, whereas ammonium sulfate provides the direct mode-specific validation.

"The performance and interpretation of the system are evaluated through four complementary analyses. First, the optical response is used to resolve freezing onset from subsequent bulk solidification. Second, dry ammonium sulfate particles, together with particle-free background measurements and aerosol-conditioning simulations, provide mode-specific validation of impact-initiated contact freezing and system reproducibility. Third, a physically based collision model is combined with freezing-inferred collision efficiencies and independent post-melt quartz particle observations to constrain particle collection in the actual C-ICE geometry. Finally, silver iodide is used as a benchmark material to evaluate freezing mode sensitivity and particle size dependent contact freezing." (Lines 90-96)

"Dry ammonium sulfate provides a particularly strong mode-specific validation of the C-ICE concept. Ammonium sulfate particles produce freezing between -17.7 and -14.4 °C, whereas particles entering the water droplet subsequently dissolve and cannot persist as conventional solid immersion mode INPs. Their corresponding aqueous droplets are expected, based on previous studies, to freeze homogeneously only at temperatures approximately 20 °C lower. These measurements therefore provide direct and mode-specific evidence that C-ICE can generate and detect impact-initiated contact freezing under stable and reproducible experimental conditions. Particle-droplet collision efficiency is constrained using three complementary levels of information. A physically based model provides CE_{model}, freezing statistics from DMA selected 200 and 800 nm AgI yield experimentally inferred CE_{exp}, and these constraints are combined to construct the observation-constrained efficiency $CE_{constr.}$ Independent post-melt observations of retained quartz particles further demonstrate substantial particle collection in the actual C-ICE geometry and provide an experimental evaluation of the resulting collision framework. AgI benchmark measurements additionally show that C-ICE resolves particle size effects, with T_{50} increasing from -12.6 °C for 200 nm particles to -12.0 °C for 800 nm particles and -10.1 °C for the polydisperse aerosol. Complementary immersion freezing measurements reveal a strong dependence on AgI loading and demonstrate why quantitative comparisons between contact and immersion modes require careful matching of particle exposure and interaction history." (Lines 637-651)

Specific comments:

1. Line 33 and throughout the manuscript: "freezing" involves per definition liquid water. So, "deposition

freezing" should be revised to "deposition nucleation". If the authors want to stress the involvement of liquid water, they should directly refer to "pore condensation and freezing".

We thank you for this comment and have replaced "deposition freezing" with "deposition nucleation" where applicable.

2. Line 156: what is meant by "grid points" in this context?

We have clarified that the grid points are the discrete temperature values at which the cumulative frozen fraction is evaluated. The temperature increment is selected adaptively, is no smaller than 0.1 °C, is an integer multiple of 0.1 °C, and is chosen to provide at least 10 points across the observed freezing range whenever possible.

3. Lines 219–223: "Under the controlled laboratory conditions of C-ICE, such particle-droplet collisions are theoretically predictable controllable and repeatable, as demonstrated in the Results section below. This approach provides a foundation for interpreting contact freezing measurements and for guiding future efforts to parameterize contact freezing in atmospheric models.": This statement is in harsh contrast to lines 505–509, where it is stated: "It is important to emphasize that the effective particle collision rates shown in Fig. 7b represent conservative lower-bound estimates, because $CEbest$ is constructed as a lower envelope constrained by experimental measurements at 200 nm and 800 nm (Sect. 3.3)." Such contradictions need to be removed. The capabilities of the new setup should be assessed realistically throughout the manuscript.

The reviewer's point is well taken. We have removed the contradictory "lower-bound" formulation, and the terms CE_{best}, CE_{min}, and CE_{max} are no longer used. The revised manuscript now clearly distinguishes the physically modeled collision efficiency from the experimentally inferred constraints and states that particle collection in C-ICE can be physically modeled and experimentally constrained, rather than fully predicted. Independent observations of quartz particles retained in the target droplet provide an additional experimental evaluation of particle collection in the actual C-ICE geometry.

"Under the controlled laboratory conditions of C-ICE, the collision process can be physically modeled and experimentally constrained, as demonstrated in the Results section below." (Lines 252-254)

"In this section, we combine the physically based collision model described in Sect. 2.3 with experimental constraints from size-selected AgI measurements and direct observations of quartz particle features retained in the target droplet after freezing and melting to derive an observation-constrained collision efficiency for C-ICE." (Lines 438-440)

"To reconcile model predictions with experimental constraints, we define three CE scenarios in Figs. 6 and S7. CE_{model} represents the physically modeled collision efficiency without observational adjustment. CE_{upper} represents the idealized upper limit in which all nozzle-delivered particles collide with the target droplet. The observation-constrained collision efficiency, CE_{constr}, incorporates the experimentally derived constraints at 200 and 800 nm while retaining the physical size dependence predicted by the model. Between the two anchor sizes, the empirical constraint is linearly interpolated; outside this range, it is extended at the nearest constrained value, while CE_{model} is retained wherever it

predicts a larger efficiency. Thus, CE_{constr} provides a smooth and system-specific representation that reconciles the physically modeled size dependence with the experimentally observed C-ICE response." (Lines 497-504)

4. Lines 290–293: "In immersion or deposition freezing experiments, grayscale-based analyses typically identify the temperature of complete freezing, which reflects bulk solidification of the droplets and is appropriate when nucleation occurs throughout the liquid or vapor phase (Kiselev et al., 2017; Thornton et al., 2023; Thompson et al., 2025)": None of the indicated references describes a grayscale-based analysis in detail. A reference that would be better suited is Miller et al. (2021). Moreover, I am not aware of any technique that uses a grayscale-based analysis for deposition nucleation. Please give a suitable reference for such an instrument or remove "deposition freezing".

   We thank you for pointing this out. We agree that the original statement was inaccurate. We have removed the statement that grayscale-based analysis is typically used in immersion or deposition nucleation experiments and no longer refer to deposition nucleation in this context. We have also added Miller et al. (2021) as suggested. The revised text now makes the narrower distinction relevant to C-ICE: many droplet freezing experiments identify freezing from the pronounced optical change associated with bulk solidification, whereas C-ICE resolves the earliest detectable liquid-to-ice transition separately from the subsequent bulk freezing process.

   "The use of the onset freezing temperature is physically motivated by the distinction between the initial ice nucleation event and subsequent bulk ice propagation. In many droplet freezing experiments, the freezing temperature is identified from the pronounced optical change associated with bulk solidification of the droplet (Thornton et al., 2023; Thompson et al., 2025; Miller et al., 2021). For C-ICE, however, resolving the earliest detectable liquid-to-ice transition is particularly important because contact freezing is initiated locally at or near the particle-droplet interface, often involving a solid-liquid-air contact line (Yang et al., 2019; Rosky et al., 2023)." (Lines 323-328)

5. Lines 344–370: In this paragraph, the performance of the dehumidifier at -15°C is discussed. Is the dehumidifier kept at this temperature throughout a cooling ramp? If yes, what are the consequences when the stage is at higher or lower temperature? Is there still time for the particle flow to equilibrate with the stage temperature and humidity before it reaches the droplet? Please clarify.

   This point has been clarified throughout Sect. 2.1, Sect. 3.2, and the Fig. 4 caption. The dehumidifier setpoint is held constant within an experimental series and does not track the cold-stage ramp. The -15 °C example is only representative. The purpose of the dehumidifier is to establish a dry and reproducible particle-laden flow and to thermally condition the gas and particles toward a selected temperature before delivery; it is not intended to force the aerosol stream to equal the instantaneous droplet temperature throughout the ramp.

   "Figure 4 illustrates the thermodynamic evolution of water vapor within the dehumidifier section of the C-ICE system for a representative operating condition." (Lines 395-396)

   "Under representative operating conditions (25 °C inlet temperature, 10% initial RH, and 1.5 L min^{-1} flow rate), the gas temperature decreases smoothly toward the selected conditioning temperature (-

15 °C), crossing 0 °C within 0.15 m of the inlet. The -15 °C setpoint represents one representative conditioning scenario rather than a universal operating temperature for all C-ICE experiments." (Lines 397-400)

"At the outlet, the aerosol particles and nitrogen carrier gas have been both dried and thermally conditioned toward the selected setpoint before entering the cold stage. Because the dehumidifier temperature is fixed during an experimental series while the cold-stage temperature continues to decrease, the conditioned aerosol stream is not necessarily at the same instantaneous temperature as the target droplet. The dehumidifier provides a reproducible and sufficiently dry thermodynamic state prior to particle delivery. Together with the continuous dry nitrogen purge of the cold-stage chamber, this conditioning suppresses widespread background condensation while allowing localized aerosol-flow-induced and freezing-induced breath figures to remain readily distinguishable." (Lines 404-410)

"The simulation is performed for an inlet airstream at room temperature (25 °C), an initial RH of 10%, a flow rate of 1.5 L min^{-1}, and a representative dehumidifier coolant setpoint of -15 °C. The -15 °C condition illustrates one typical operating scenario and does not represent a universal setpoint for all C-ICE experiments. The dehumidifier temperature is selected according to the aerosol material, expected freezing temperature range, and drying requirements and is held constant within a given experimental series." (Lines 417-421)

6. Lines 438–452 (adjustment of collision efficiency to experimental values): the experimentally derived collision efficiencies for 200 nm and 800 nm particles are considered here a lower limit (a "lower envelope" as stated on line 441) assuming that one collision triggers freezing. Yet, the collision efficiency might also be much higher with an upper limit of 1, or even lower if freezing occurred via immersion mode on previously collected particles. Therefore, the uncertainty is even larger than discussed. This uncertainty also needs to be acknowledged in the conclusion and in the abstract of the paper.

We thank you for this comment.

The revised manuscript no longer labels the freezing-inferred values as lower limits. They are denoted as CE_{exp} and treated only as empirical constraints under the stated assumption. $CE_{upper} = 1$ is shown explicitly, and CE_{constr} is constructed by combining CE_{model} and the CE_{exp} anchor points. Independent quartz observations provide an additional experimental evaluation. The abstract and conclusions have also been revised.

"Collision efficiency is constrained by combining a physically based model with freezing-inferred experimental efficiencies. Independent post-melt observations of retained quartz particles further validate particle collection in the actual C-ICE geometry and support the resulting observation-constrained collision efficiency." (Lines 26-28)

"In summary, the physically based CE_{model}, the size-resolved AgI constraints, and the independent quartz collection measurements provide a consistent experimental basis for CE_{constr}. This observation-constrained efficiency is subsequently used to convert measured aerosol number concentrations and size distributions into effective particle collision rates onto the target droplet." (Lines 539-542)

"Particle-droplet collision efficiency is constrained using three complementary levels of information.

A physically based model provides CE_{model}, freezing statistics from DMA selected 200 and 800 nm AgI yield experimentally inferred CE_{exp}, and these constraints are combined to construct the observation-constrained efficiency CE_{constr}. Independent post-melt observations of retained quartz particles further demonstrate substantial particle collection in the actual C-ICE geometry and provide an experimental evaluation of the resulting collision framework." (Lines 642-647)

7. Lines 491–492: what is the definition of the median effective particle nucleation rate?

We appreciate your comment.

The quantity is an effective particle collision rate, not a particle nucleation rate. It is defined as the number of particles predicted to collide with the target droplet per second and is calculated from the measured aerosol number concentration, the aerosol flow rate, and CE_constr. For the 200 and 800 nm AgI cases, the median effective collision rate is 0.17 s^{-1} for both populations.

"(b) Effective particle collision rate onto the target droplet for the same experiments shown in panel (a), expressed as the number of particles colliding with the droplet per second. The collision rate is calculated by combining measured aerosol number concentrations (from CPC and OPC measurements) with the observation-constrained collision efficiency (CE_{constr}) and the aerosol flow rate (120 cm^3 min^{-1})." (Lines 606-609)

"To help interpret the differences among the frozen fraction results, Fig. 9b presents the effective particle collision rate onto the target droplet, expressed as the number of particles colliding with the droplet per second. Rates are calculated from measured aerosol number concentrations (CPC and OPC) combined with the observation-constrained collision efficiency CE_{constr} (Sect. 3.3) and the known aerosol flow rate. The median effective particle collision rate is 0.17 s^{-1} for both 200 nm and 800 nm populations, with corresponding mean rates of 0.20 s^{-1} and 0.29 s^{-1}, respectively (Table S5). Thus, the warmer freezing of the 800 nm particles occurs under comparable particle-delivery rates, further supporting a particle-size dependence of the AgI freezing response." (Lines 612-618)